Progress In Electromagnetics Research B, Vol. 65, 65–80, 2016

Miniaturized Slotted Ground UWB Antenna Loaded with Metamaterial for WLAN and WiMAX Applications

Ritesh Kumar Saraswat[1, *] and Mithilesh Kumar[2]

Abstract—This paper presents a miniaturized ultra wideband (UWB) antenna with metamaterial for WLAN and WiMax applications. For miniaturization of UWB antenna resonating 3.1–10.6 is designed Ghz using fractalization of the radiating edge and slotted ground structure approach. A miniaturization of active patch area and antenna volume is achieved up to 63.48% and 42.24% respectively, with respect to the conventional monopole UWB antenna. This antenna achieves a 143% impedance bandwidth covering the frequency band from 2.54 GHz to 15.36 GHz under simulation and 132% (2.95–14.28 GHz) in measurement. The electrical dimension of this antenna is $0.32\lambda \times 0.32\lambda$ (38 mm×38 mm) at lower frequency of 2.54 GHz. As per IEEE 802.11a/b/g and IEEE 802.16e standards, WLAN (2.4–2.5 GHz, 5.150–5.250 GHz, 5.725–5.825 GHz), WiMAX (3.3–3.8 GHz) bands are achieved by using slotted ground structure and metamaterial rectangular split ring resonator. The proposed antenna is fabricated on FR4 substrate of thickness 1.6 mm and a dielectric constant 4.3 and tested. The proposed antenna yields a −10 dB impedance bandwidth of about 11.1% (2.39–2.67 GHz), 59.1% (2.87–5.28 GHz) and 7.4% (5.58–6.01 GHz) under simulation and 4.5% (2.41–2.52 GHz), 51.1% (3.12–5.26 GHz) and 3.8% (5.69–5.91 GHz) in measurement for 2.4, 3.5 & 5 and 5.8 GHz bands respectively. Stable radiation patterns with low cross polarization, high average antenna gain of 3.02 dBi under simulation and 2.14 dBi in measurement and measured peak average radiation efficiency of 76.6% are observed for the operating bands. Experimental results seem in good agreement with the simulated ones of the proposed antenna.

1. INTRODUCTION

In recent years, with the rapid development in wireless communications, many efforts are devoted to reduce the size of microstrip antennas. For this purpose, several methods have been proposed, such as using a dielectric substrate of high permittivity, Defected Microstrip Structure (DMS), Defected Ground Structure (DGS) at the ground plane or a combination of them [1–3]. In present time, wireless communication systems are significantly popular. There have been ever growing demands for antenna designs that possess the following highly desirable attributes: compact size, low cost, high performance, multi-band [4] etc. Variety of approaches are available that have been evolved over the last few decades and utilized for achieved the design targets. Recently, due to the use of fractal concept the possibility of developing antenna design objective has been improved. With the introduction of fractal shapes of radiating element in antenna engineering, the multiband resonance with single antenna, becomes attractive [4, 5]. The respective term fractal was introduced by B. B. Mandalbrot and later followed by many researchers in investigating in the field of miniaturized antenna design [6, 7]. In modern wireless communication systems, multiband antennas play an important role. The challenges, however, include miniaturization, impedance matching, low profile, low cost and integration with RF circuits. A necessity of wireless communication systems is the multiple utilization of communication standards in

Received 27 November 2015, Accepted 27 December 2015, Scheduled 5 January 2016
* Corresponding author: Ritesh Kumar Saraswat (ritesh.saraswat9@gmail.com).
[1] M.L.V. Govt. Textile & Engineering College, Bhilwara (Rajasthan), India. [2] Rajasthan Technical University, Kota (Rajasthan), India.

a single system. To integrate different wireless communication standards in a single portable antenna system, various narrow band, wideband, ultra-wideband (UWB), dual-band and multiband, antennas are developed [8–11]. However, to mitigate the electromagnetic interference (EMI) due to existence of other nearby communication systems, the multiband antennas are preferred over ultra-wideband antennas. Several low profile and compact size dual band antennas are proposed for wireless local area network (WLAN) applications. These respective antennas, however, are limited to only WLAN standards [12–15]. In general, by modifying radiating patch or ground plane by adding multi-branched strips and etched slots, multiband resonant modes can be achieved. Using the fractal concepts and band notched characteristics, the multiband resonance with single antenna can be obtained. These antennas incorporate both WLAN and microwave access (WiMAX) standards with wide band coverage and good radiation characteristics [16–21]. The proposed multiband metamaterial antennas are focus on miniaturization, better radiation performance, optimum bandwidth and gain enhancement [22–25]. The split ring resonators (SRRs) based monopole antennas [26], SRRs and complementary split ring resonators (CSRRs) loaded substrates [27, 28] and partial metamaterial loading [29] are the metamaterial inspired techniques used in antenna design.

In present work, firstly the conventional UWB antenna is miniaturized with respective active patch area and volume of antenna by implementing the fractalization of patch and by reducing the antenna dimensions (length and width). As per the proposed design, the evolution of UWB antenna resonates in 3 modes such as; 2.45–14.42 GHz (142%) for conventional, 2.58–14.38 GHz (139%) for fractal and 2.54–15.36 GHz (143%) for miniaturized. The proposed miniaturized UWB antenna achieved impedance bandwidth of 143% (2.54–15.36 GHz) under simulation and 132% (2.95–14.28 GHz) in measurement.

This followed a partial metamaterial loading by introducing modified rectangular SRR with octagonal shape radiating patch and by using slotted ground structure approach and obtained the WLAN and WiMAX frequency bands 2.39–2.67 GHz (11.1%), 2.87–5.28 GHz (59.1%) and 5.58–6.01 GHz (7.4%) under simulation and 2.41–2.52 GHz (4.5%), 3.12–5.26 GHz (51.1%) and 5.69–5.91 GHz (3.8%) in measurement.

For these respective bands, the peak average antenna gain of 3.02 dBi under simulation and 2.14 dBi in measurement are observed. The high average measured radiation efficiency of 76.6% is obtained and also observed that the efficiency stays above 70% in all the operating bands of the WLAN and WiMAX applications. The negative permeability characteristic of rectangular SRR is utilized to achieve the multi-resonant property of the proposed antenna. It uses metamaterial rectangular SRR to cover WLAN and WiMAX standards and has miniaturization with respect to the active patch area and volume of antenna. The CST Microwave Studio (CST MWS) software [30] is used for simulation while the measurements are taken using a E5071C (300 kHz–20 GHz) ENA series Agilent Technologies Vector Network Analyzer.

The proposed antenna is fabricated with the help of PCB prototype machine Caddo-71. In the following section, the geometry of miniaturized ultrawide band (UWB) antenna is described with simulated and measured results of reflection coefficients, gain and radiation efficiency. Next describes the configuration of proposed antenna with analysis of effective permeability of proposed rectangular SRR from S-parameters. The proposed antenna design is described, and the gain, radiation efficiency and radiation patterns are discussed. Finally, conclusions are made.

2. MINIATURIZED ULTRAWIDEBAND (UWB) ANTENNA DESIGN

Initially, an octagonal shape UWB antenna is designed on the basis of its operability over wide bandwidth and good radiation characteristics. Miniaturizing of existing antenna leads to improvement in overall performance with special reference to its applicability. In the present design miniaturization of UWB monopole antenna configuration 'a' is done by using the fractalization approach that lead to reduction in active patch area and volume of antenna structure, which is shown in configuration 'b'. As per the evolution of proposed miniaturized UWB antenna, configuration 'c' is obtain by reducing the antenna dimensions (L_S & W_S) and also reduce the active patch area by inserting the circular slot of radius of 6.5 mm, as shown in configuration 'c' of Figure 1. The reduction of active patch area and antenna volume is observed in Table 1.

The antenna is constructed on an FR4 substrate ($38\times38\,\text{mm}^2$) with the relative permittivity 4.3

Table 1. Analysis of UWB antenna miniaturization carried out as per design evolution.

Parameter	Conventional UWB Antenna	Fractal UWB Antenna	Proposed UWB Antenna	% Reduction (with respect to conventional UWB antenna)
Active Patch Area (in mm^2)	482.84	263.99	176.35	63.48
Volume of antenna (in mm^3)	4000	2752	2310.4	42.24

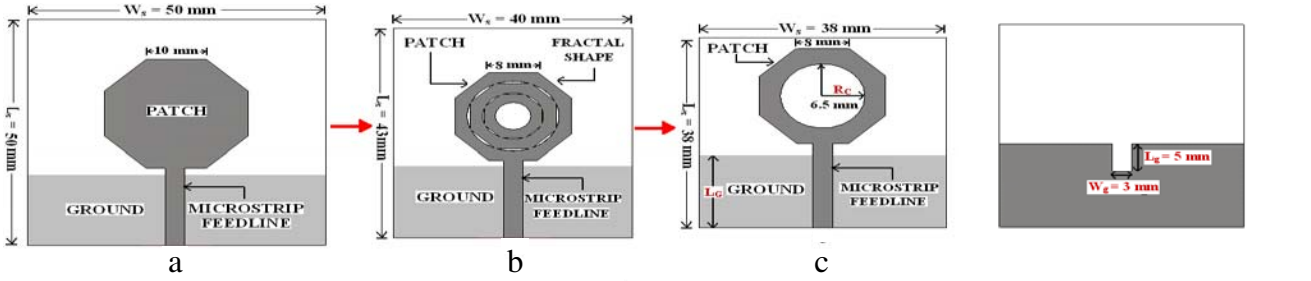

(a) Front view of structure (b) Back view of proposed structure 'c'

Figure 1. Evolution of the proposed UWB monopole antenna.

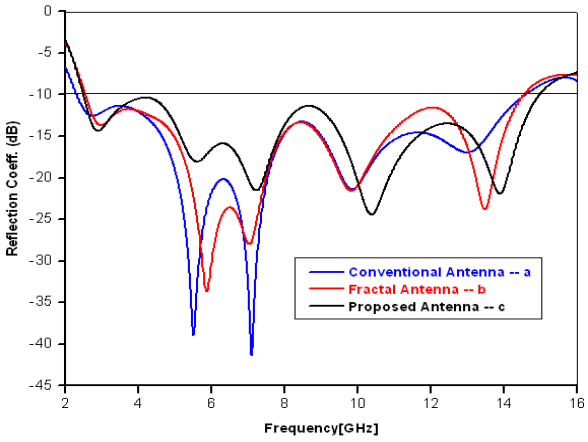

Figure 2. Simulated reflection coefficient S_{11} of the UWB antenna for configuration a, b & c in Figure 1.

and thickness 1.6 mm. The radiating element is a octagonal shape patch of branch length 8 mm with circular slot of radius 6.5 mm, which is fed with a 50 ohm microstrip feed line with the length of 17 mm and width of 3.16 mm. On the bottom of the substrate, there is a ground plane with $15.5\times38\,mm^2$ dimensions and height 0.01 mm, below the microstrip feed line. The circular slot makes a portion of area 132.66 mm^2 from the octagonal shape of patch of area 309.02 mm^2 as shown in configuration 'c' in Figure 1.

At the optimized value of antenna dimensions, the input reflection coefficient S_{11} of UWB antenna for configuration a, b & c is below -10 dB with impedance bandwidth of 142% (2.45–14.42 GHz), 139% (2.58–14.38 GHz) and 143% (2.54–15.36 GHz) respectively under simulation, shown in Figure 2.

From Figure 2, it is clear that these three configurations a, b & c of UWB antenna have almost the same operating frequency range, and they offer similar impedance bandwidth. It is observed that the

proposed antenna configuration 'c' requires smaller size than the conventional octagonal shape patch antenna. The reductions in patch size and antenna volume are about 63.48% and 42.24%, respectively, as shown in Table 1. So the miniaturization of UWB antenna is successfully carried out as per the design evolution in Figure 1.

The parametric study of the proposed UWB antenna reveals the variation in antenna performance with change in ground length L_G and radius of circular slot R_C of the octagonal shape patch which is shown in Figure 3. As seen, by varying the ground length (length L_G from 15 to 16.25 mm) and radius of circular slot (radius R_C from 5.5 to 7.5 mm), the impedance matching with UWB is achieved at length $L_G = 15.5$ mm and radius $R_C = 6.5$ mm.

It is also observed from Figure 3 that the impedance matching is improved at lower frequencies (2–4 GHz) when the ground length and radius of circular slot are increased (either by increasing L_G or R_C) whereas at higher frequencies (above 5 GHz) it is improved when the ground length and radius of circular slot are reduced.

Antenna performance is analyzed by varying the dimensions of ground slot (length L_g from 4.25

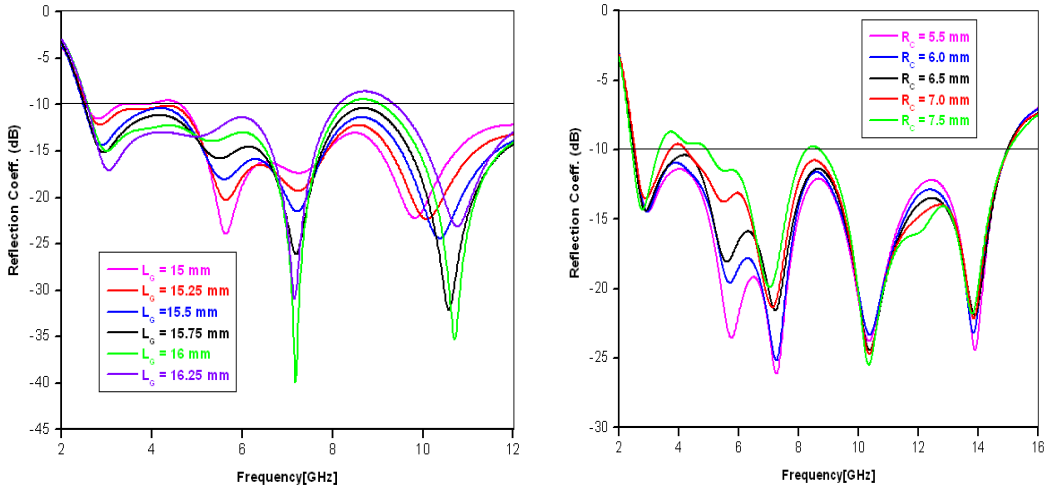

Figure 3. Simulated reflection coefficient S_{11} of antenna 'c' for different values of L_G and R_C.

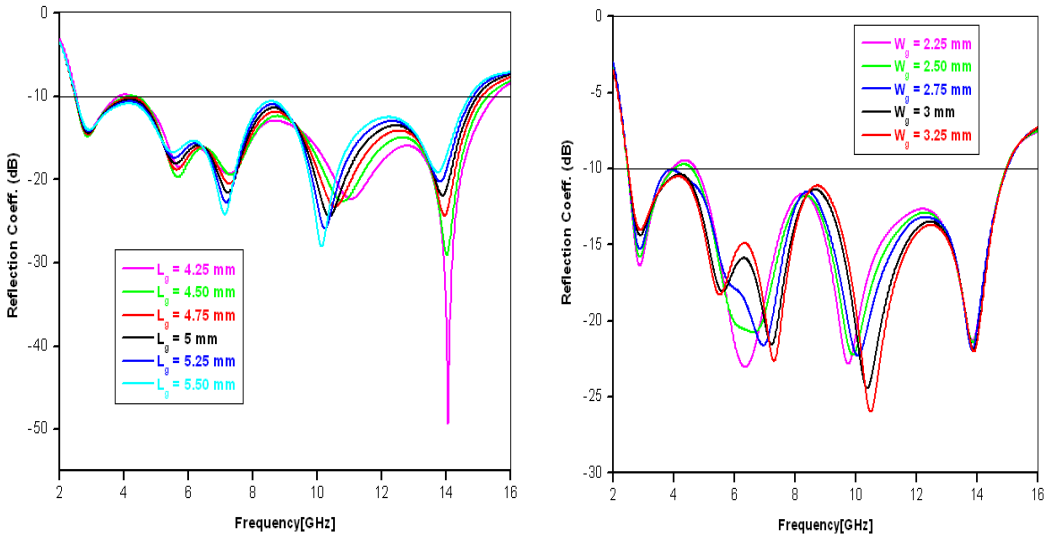

Figure 4. Simulated reflection coefficient S_{11} of antenna 'c' for different values of L_g and W_g.

to 5.50 mm and width W_g from 2.25 to 3.25 mm). The impedance matching with UWB is obtained at length $L_g = 5$ mm and width $W_g = 3$ mm as shown in Figure 4. Moreover, the bandwidth of proposed UWB antenna is controllable by changing the length L_g and width W_g of ground slot (in Figure 1(b)). By the variations of these slot dimensions, impedance bandwidth changes accordingly, as shown in Figure 4. By increasing the slot length L_g and width W_g, bandwidth of the antenna decreases from 34% to 12% in proposed structure. From Figure 4 it is also observed that the impedance matching is improved at lower frequency (2–6 GHz) when the slot dimensions are reduced (either by reducing L_g or W_g) whereas at higher frequencies (above 8 GHz) it is improved when slot dimensions are increased. Finally, the variation in the UWB impedance bandwidth with variation in the slot dimensions indicates the presence of optimal values for the best performance.

At the optimized value of $L_G = 15.5$ mm, $R_C = 6.5$ mm, $L_g = 5$ mm and $W_g = 3$ mm, the input reflection coefficient S_{11} of proposed antenna 'c' is below -10 dB with impedance bandwidth of 143% (2.54–15.36 GHz) under simulation and 132% (2.95–14.28 GHz) in measurement, shown in Figure 5.

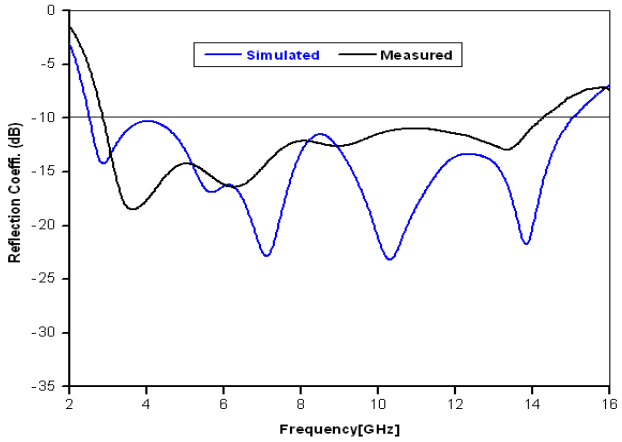

Figure 5. Simulated and measured reflection coefficient S_{11} of the proposed UWB antenna 'c'.

3. PROPOSED ANTENNA CONFIGURATION

In this section we analyze the design evolution of miniaturized UWB antenna with proposed SRR for WLAN and WiMAX applications. The proposed miniaturized UWB monopole antenna (from previous section) can be reconfigured to other frequency bands of WLAN and WiMAX by implementing the slotted ground structure and proposed rectangular SRR, as shown in configuration 'c' of Figure 6. The proposed antenna structure consists of a miniaturized octagonal shape with proposed SRR as the radiating element, a 50 ohm feed line, and slotted ground plane with two slots.

An inverted U type slotted structure created in the ground of the proposed antenna acts as a filter, which is designed to suppress the frequencies outside the desired frequency band. The observation is done on the proposed antenna by considering the case with and without inverted U slot on ground plane. Figure 7 represents the simulated input reflection coefficient S_{11} of proposed antenna for three cases, where in case-I of without proposed SRR and inverted U type slot on ground it achieved UWB range 2.54–15.36 GHz (143%), for case-II of without proposed SRR and with inverted U type slot on ground it achieved dual bands 2.82–4.71 GHz (50%) & 5.78–6.62 GHz (13%) and for case-III of with proposed SRR and inverted U type slot on ground it achieved triple bands 2.39–2.67 GHz (11.1%), 2.87–5.28 GHz (59.1%) and 5.58–6.01 GHz (7.4%).

The input reflection coefficient S_{11} of antenna with the proposed SRR is below -10 dB with impedance bandwidth of 51.1% (2.26–3.81 GHz), 6.5% (4.01–4.28 GHz) and 5.6% (5.71–6.04 GHz) for configuration 'a', 52.2% (2.31–3.94 GHz) and 6.0% (4.82–5.12 GHz) for configuration 'b' and 11.1% (2.39–2.67 GHz), 59.1% (2.87–5.28 GHz) and 7.4% (5.58–6.01 GHz) for configuration 'c' to cover WLAN & WiMAX bands under simulation respectively, shown in Figure 8.

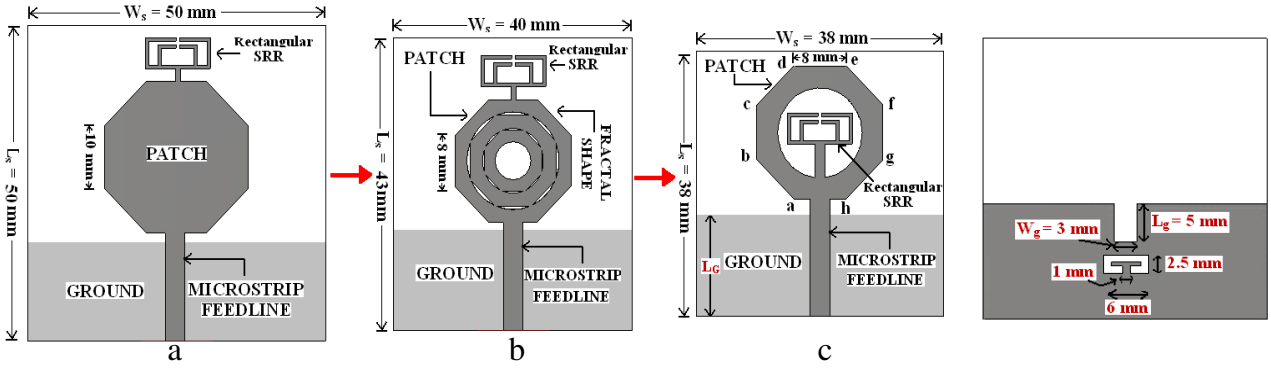

(a) Front view of structure (b) Back view of proposed structure 'c'

Figure 6. Design Evolution of the proposed monopole antenna.

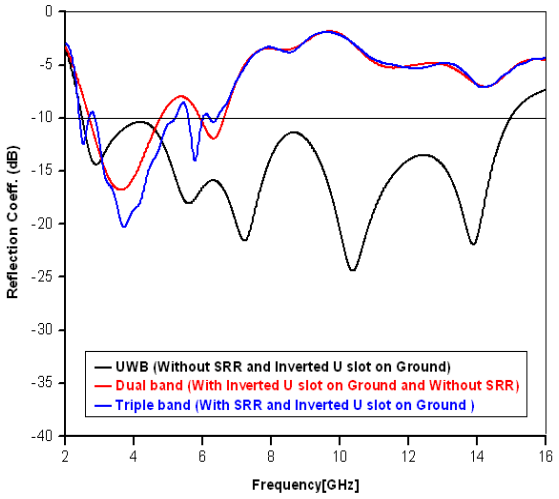

Figure 7. Simulated reflection coefficient S_{11} of the antenna for case I, II & III.

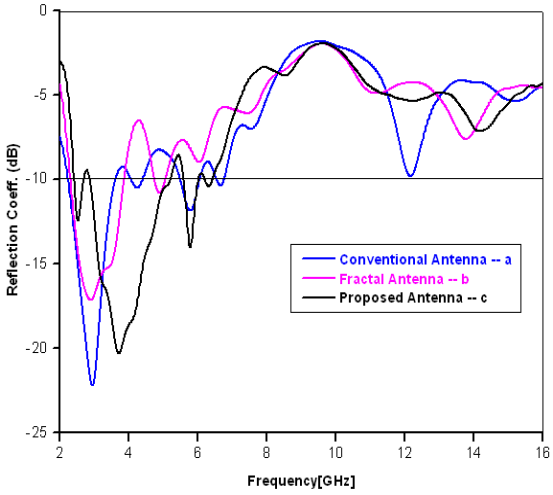

Figure 8. Simulated reflection coefficient S_{11} of the antenna for configuration a, b & c in Figure 6.

Respective rectangular SRRs are made of one or more conducting rings on a dielectric substrate with slits etched opposite to each other. The usual rectangular SRR is modified in such a way that keeping a common loop on one side and both the splits on the other side as shown in configuration 'a' in Figure 9. The geometry with dimensions of the proposed antenna is further illustrated in Figure 9 with details and a side view and bottom view.

The proposed antenna is initially simulated on CST Microwave Studio (MWS) software [30] and then fabricated with the optimized dimensions, on a low cost FR4 substrate with dielectric constant $\varepsilon_r = 4.3$, thickness $h = 1.6$ mm and loss tangent, $\tan\delta$ about 0.025, as shown in Figure 10.

Figure 11 shows the measurement setup for proposed antenna to obtain the measured reflection coefficient by using vector network analyzer (VNA) and radiation characteristics with the help of anechoic chamber.

Initially, an octagonal shape UWB antenna is designed and subsequently redesigned by implementing slotted ground approach from Figure 9(c), achieving dual bands with impedance bandwidth of 50% (2.82–4.71 GHz) and 13% (5.78–6.62 GHz) as shown in Figure 12 (blue line). When a rectangular split ring resonator (SRR) structure is loaded with octagonal shape patch, it creates a triple band in place of existing dual band antenna system. In triple band mode of proposed antenna with rectangular SRR, 10 dB impedance bandwidth achieved is 11.1% (2.39–2.67 GHz), 59.1% (2.87–5.28 GHz) and 7.4% (5.58–6.01 GHz) under simulation whereas 4.5% (2.41–2.52 GHz), 51.1% (3.12–

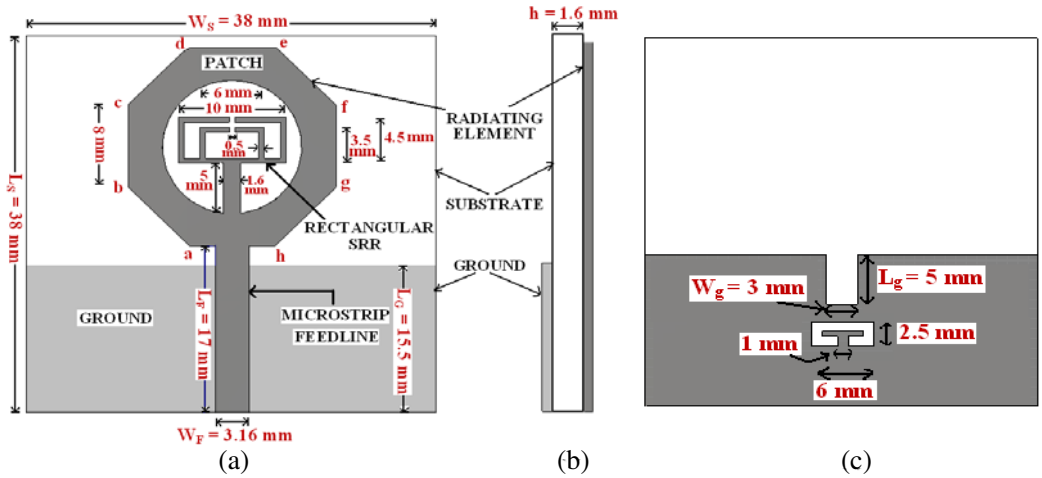

Figure 9. Configuration of the proposed antenna: (a) Front view of structure; (b) Side view of structure; (c) Back view of structure.

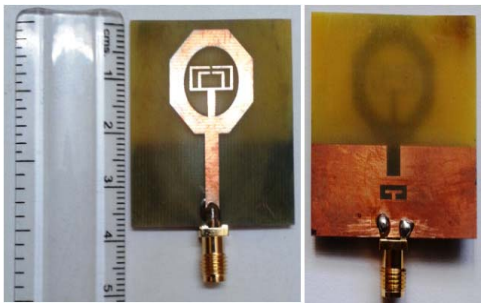

Figure 10. Image of the fabricated split ring loaded triple band antenna '*c*': (a) top view; (b) bottom view.

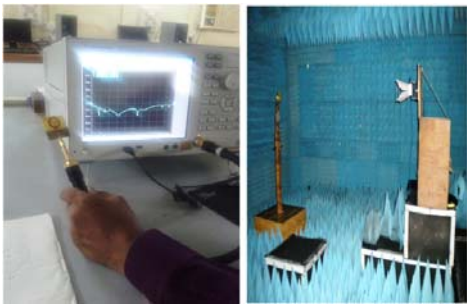

Figure 11. Images of measurement setup for proposed antenna.

5.26 GHz) and 3.8% (5.69–5.91 GHz) in measurement as shown in Figure 12. As compared to the simulated result in case of "without rectangular SRR" with the measured result in case of "with rectangular SRR" show that this has caused a 9.8% decrease in fundamental resonance bandwidth. A 6.6%, 8% and 3.6% decrease in measured bandwidth at the first, second and third resonant band are observed respectively. This may be attributed to thick soldering of SMA connector and fabrication tolerance. However, the proposed triple band antenna has sufficient bandwidth that clearly meets the requirement of WLAN and WiMAX standards.

As seen in Figure 12, in the case of "without rectangular SSR", the WiMAX band (3.3–3.8 GHz) [59.1% (2.87–5.28 GHz) under simulation and 51.1% (3.12–5.26 GHz) in measurement] and upper WLAN band (5.150–5.250 & 5.725–5.825 GHz) [7.4% (5.58–6.01 GHz) under simulation and 3.8% (5.69–5.91 GHz) in measurement] of proposed antenna is achieved by introducing slots on ground plane. These slots perturb the current flow in antenna structure, creating an additional current path that leads to the dual band operation. A parametric study is carried out to examine the effects of added slots as shown in Figure 13. It is observed that with increasing the slot dimensions (either slot length L_g or width W_g), the lower resonant band shifts towards lower frequencies. The impedance matching is improved at lower resonance when the slot dimensions are reduced whereas at upper resonance when the slot dimensions are increased. Therefore, the desired dual band performance is obtained with an optimum slot length of 5 mm and width of 3 mm to operate in both bands simultaneously.

To ensure good impedance matching, the antenna performance is studied with change in ground length L_G and radius of circular slot R_C of the octagonal shape patch (in Figure 1), shown in

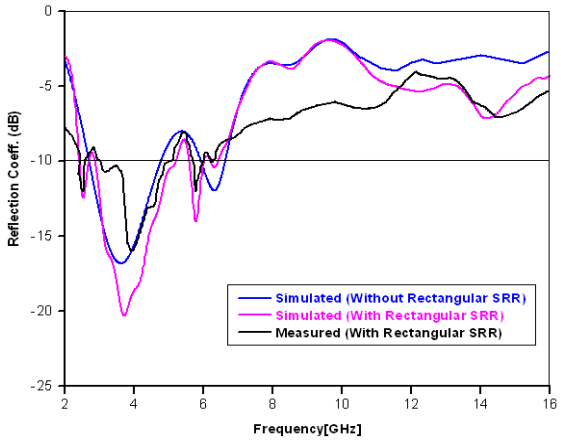

Figure 12. Simulated and measured reflection coefficient S_{11} of the proposed antenna with and without the rectangular SRR.

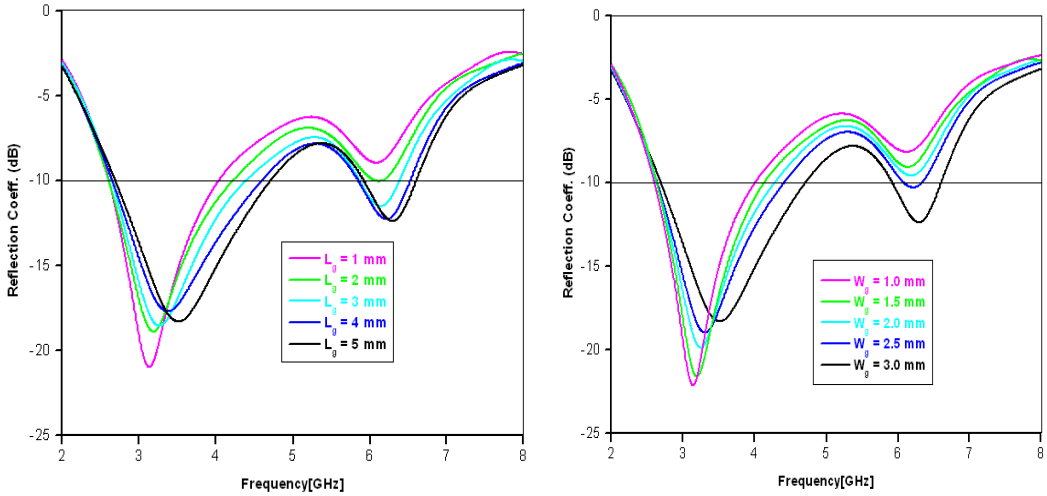

Figure 13. Simulated reflection coefficient S_{11} of proposed antenna (without rectangular SRR) for different values of L_g and W_g.

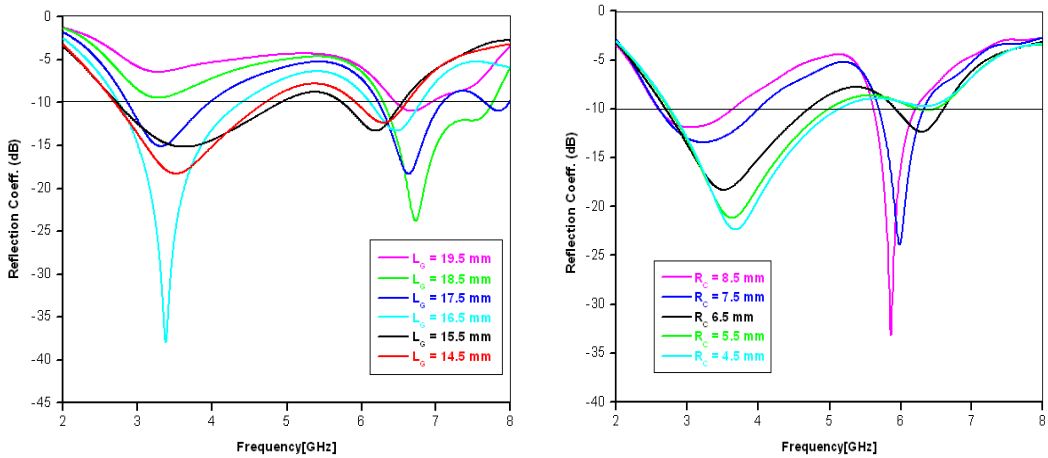

Figure 14. Simulated reflection coefficient S_{11} of proposed antenna (without rectangular SRR) for different values of L_G and R_C.

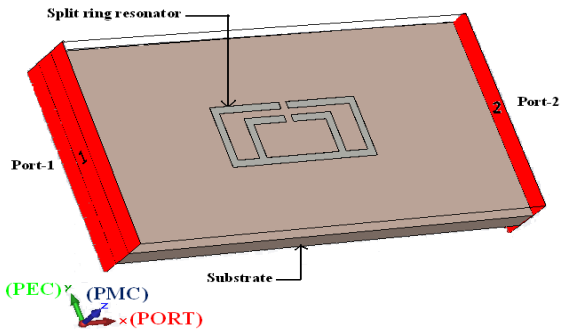

Figure 15. Simulation setup to retrieve S-parameters (S_{11} and S_{21}).

Figure 14. As observed, by varying the ground length dimensions (length L_G from 19.5 to 14.5 mm) and radius of circular slot (radius R_C from 8.5 to 4.5 mm), the impedance matching is achieved at length $L_G = 15.5$ mm and radius $R_C = 6.5$ mm. It is also observed from Figure 14 that the impedance matching is improved at lower frequencies (3–4 GHz) when the ground length dimensions and radius of circular slot are reduced (either by reducing L_G or R_C) whereas at higher frequencies (above 5.5 GHz) it is improved when the ground length dimensions and radius of circular slot are increased.

In order to achieve the WLAN frequency band (2.4–2.5 GHz), a rectangular SRR is introduced with patch element, where the split induces solenoidal currents with a time varying magnetic field. It, in turn, generates a magnetic response from the conductor. The physical parameters (length, width, split gap) of the proposed rectangular SRR are optimized to obtain resonance at the WLAN frequency band (2.4–2.5 GHz).

Determination of effective permittivity and permeability of the proposed rectangular SRR from S-parameters (S_{11} and S_{21}) is proposed by Smith et al. The parameter retrieval procedure for SRR, based on Nicholson-Ross-Weir (NRW) method, is adapted [31]. Figure 15 shows the waveguide setup to retrieve S-parameters (S_{11} and S_{21}) which is used in CST Microwave Studio (MWS) software [30] for calculating the transmission (S_{21}) and reflection coefficients (S_{11}) of the proposed SRR. For practical analysis, the rectangular SRR has to be kept inside the waveguide medium as proposed by [32]. An electromagnetic wave is incident through one port (port-1) and the corresponding reflection (S_{11}) and transmission coefficient (S_{21}) can be measured at another port (port-2) for retrieving the effective medium parameters. The transmission and reflection coefficients obtained from the waveguide environment designed in CST Microwave Studio (MWS) software [30] that is utilized to retrieve the magnetic permeability (μ).

The proposed rectangular SRR is excited by the wave ports. From these parameters, the values of refractive index (n_r) and impedance (z_s) are determined using the Equations (1) and (2) as proposed by [31, 33]. Further, the magnetic permeability is retrieved by using following equations.

$$n_r = (1/k_0 d)\cos^{-1}[(1/2S_{21})\{(1-S_{11})^2 + (S_{21})^2\}] \quad (1)$$

$$z_s = [\{(1+S_{11})^2 - (S_{21})^2\}/\{(1-S_{11})^2 - (S_{21})^2\}]^{1/2} \quad (2)$$

$$\mu = n_r \times z_s \quad (3)$$

where, $k_0 = \omega/c$. $\omega = 2\pi f$, angular frequency (radian/second). c = Speed of light (3×10^8 m/s). d = Slab thickness.

The waveguide experimental setup to retrieve S-parameters is shown in Figure 16. The setup consists of two coaxial-to-waveguide adapters which are attached to a rectangular waveguide loaded with the proposed rectangular SRR under test. This arrangement is connected to VNA (vector network analyzer) with help of cable for measurement of S-parameters. The cross section of the waveguide is completely covering the proposed SRR thickness of d. The incident, transmitted, and reflected waves are stand waves in the waveguide environment. The distances between adapters and the proposed SRR are large enough to significantly attenuate the higher order incident evanescent modes due to the coaxial-to-waveguide adapters, prior to reaching the SRR under test [32].

The simulation based S-parameters (S_{21} & S_{11}) of proposed SRR are graphically shown in Figure 17, where transmission peak occurs at 2.4 GHz. Because of magnetically resonant structure, the proposed

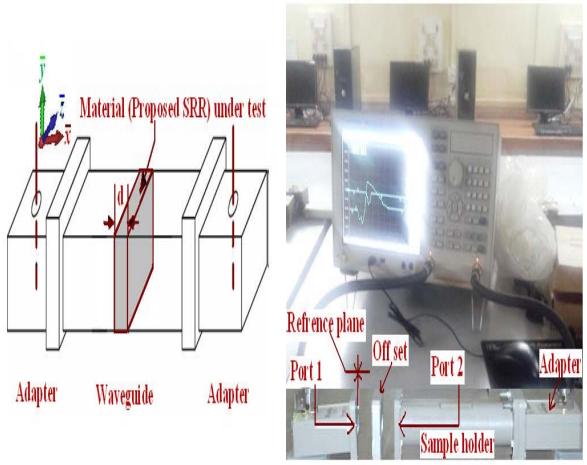

Figure 16. Waveguide setup for retrieve S-parameters [32].

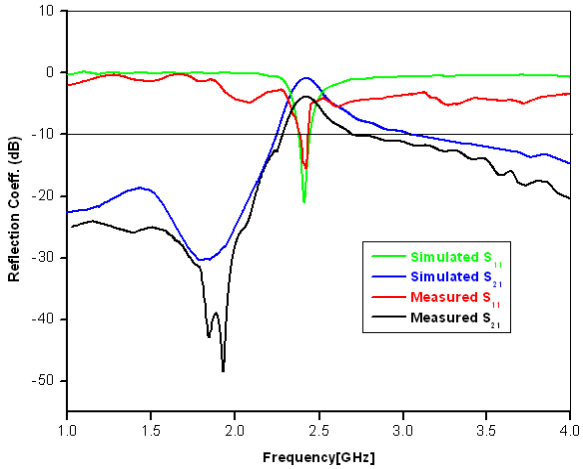

Figure 17. Simulated results of S-parameters (S_{11} and S_{21}) of proposed rectangular SRR.

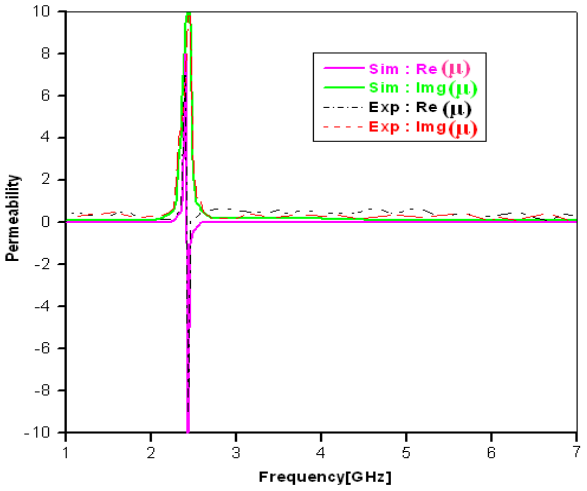

Figure 18. Extracted Negative permeability characteristics of proposed rectangular SRR.

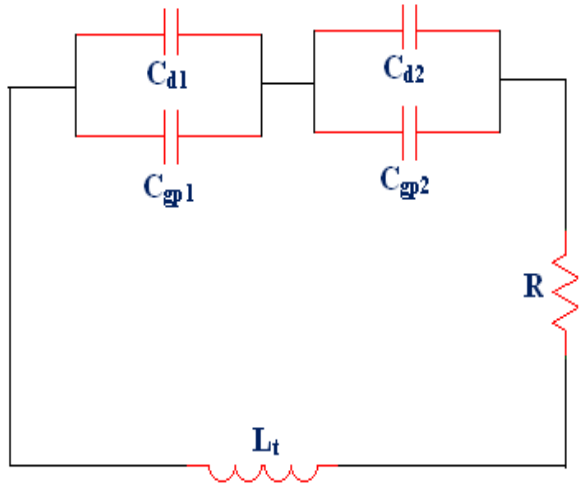

Figure 19. Equivalent circuit of the proposed rectangular SRR unit cell.

rectangular SRR induces a perpendicular magnetic field responsible for creating the negative value of permeability (μ). It represents the stop band characteristics of the SRR at the frequency of 2.4 GHz, where the reflection coefficient (S_{11}) is almost equal to zero (< -3 dB) and the transmission coefficient (S_{21}) less than -10 dB. The retrieved negative μ of the SRR is seen at 2.4 GHz as shown in Figure 18.

The equivalent circuit of the proposed SRR is shown in Figure 19, where L_t indicates the total inductance, and C_{d1} & C_{d2} are distributed capacitances which are created at the two halves of the rectangular SRR structure with respect to the split gaps [33]. This equivalent circuit also includes gap capacitances C_{gp1} and C_{gp2}. Induced electromotive force is present around the SRR because of applied an external magnetic field along z-axis of the SRR. This electromotive force creates current that passes from one rectangular ring to the other through inter-ring spacing and the structure acts as a LC resonant circuit. The resonance frequency of the proposed rectangular SRR is expressed by the following equation [33].

$$\omega L_t = (1/\omega C_t) \tag{4}$$

From Equation (4), L_t is the total inductance of the proposed SRR and can be computed according

to [33] as,

$$L_t = 0.0002[\log_{10}\{4(l_w)/d_w\} - \theta], \tag{5}$$

where l_w and d_w are the wire length and width, respectively, and the constant θ is fixed at value of 2.451 [33].

The length (circumference) of circular ring ($l_{wc} = 2\pi r$) of radius r is considered as a circumference of rectangular ring [$l_{wr} = 2(l_r + w_r)$] as shown in Figure 20 [34]. The relation between the perimeter of rectangular ring and circumference of circular ring is shown in Equation (6).

$$2(l_r + w_r) = 2\pi r \tag{6}$$

where, l_r & w_r is the length and width of rectangular ring, respectively and r the radius of circular ring.

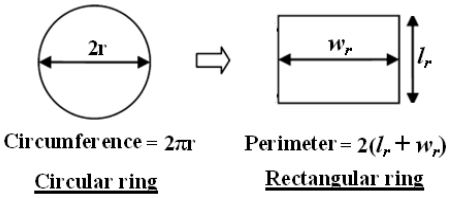

Figure 20. Schematic diagram for equating the circumference (length of wire) of circular ring with rectangular ring [34].

From Equation (4), the total equivalent capacitance, C_t of the proposed rectangular SRR, can be calculated in view of the equivalent circuit shown in Figure 19. The gap capacitance is obtained by,

$$C_{gp} = (C_{pul}/2)[\pi\{(L_{int} + W_{int})/2\pi\} - g_a] + [(\varepsilon_0 wt)/(2g_a)], \tag{7}$$

where, L_{int} (3.5 mm, from Figure 9) and W_{int} (6 mm from Figure 9) are length and width of internal rectangular ring of proposed SRR, respectively, and ε_0 is the free space permittivity. The split gap $g_a = 0.5$ mm, and t & w are thickness and width of rectangular rings, respectively. The capacitance C_{pul} denotes capacitance per unit length between the rectangular rings, and it may be calculated as follows [33],

$$C_{pul} = [(\varepsilon_e)^{1/2}/(c_0 Z_0)], \tag{8}$$

where, ε_e is the effective permittivity of the medium, $c_0 = 3 \times 10^8$ m/s the speed of light in free space, and Z_0 the impedance of the medium.

To understand the behavior of the proposed antenna's resonant modes at 2.40 GHz, 3.65 GHz and 5.82 GHz (magenta color line, Figure 12), the simulated surface current distributions of the proposed antenna configuration are shown in Figure 21. At resonant mode 2.40 GHz, current distributions are mainly observed in the feed line, the periphery of the octagonal shape patch and the rectangular SRR's

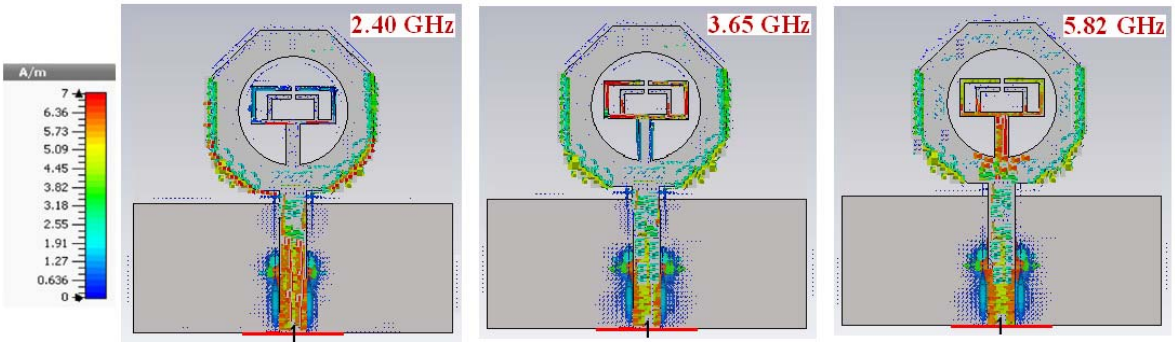

Figure 21. Simulated results of surface current distribution for the proposed antenna at different resonant frequencies.

inner ring which can be seen in Figure 21(a). As shown in Figure 21(b) for the 3.65 GHz WiMAX frequency band, current is mostly concentrated around the proposed split rings (rectangular SRR's) of the structure, which contributes to the wide band behavior 59.1% (2.87–5.28 GHz) at this frequency band. As seen in Figure 21(c), the maximum current density is observed around the strip between patch and SRR's of the antenna, for the upper WLAN frequency band at 5.82 GHz.

Figure 22 shows the 3D-gain of the proposed antenna at different resonance frequencies, which indicates the maximum radiation in direction with respective to different values of theta and phi. At higher resonant frequency 5 & 5.8 GHz, directivity is increased as compared to the lower resonant frequency at 2.4 GHz, so that gain is improved at higher resonant frequency.

The gain of the proposed antenna is calculated using gain transfer method where the horn antenna is used as the reference antenna for the measurement. Figure 23 represents the simulated and measured gains of the proposed antenna. At lower frequencies (below 3 GHz), the gain is reduced whereas at higher frequencies (above 5 GHz), the gain is improved with respect to the gain at lower frequency. The measured peak gains of 1.58, 1.75, 2.10 and 2.92 dBi are observed for 2.4, 3.5, 5 and 5.8 GHz WLAN and WiMAX frequency bands.

As per Figure 24, the radiation efficiency varies from 91.5% to 61.2% under simulation and from

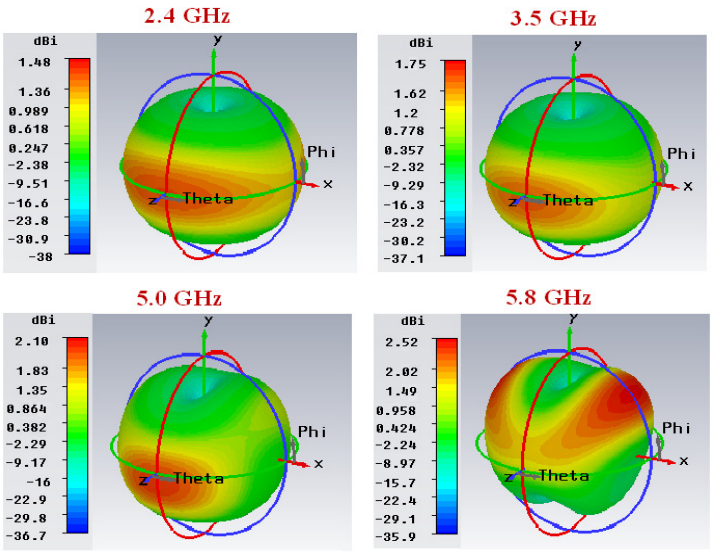

Figure 22. Simulated gain (dB) of the proposed antenna for different frequencies.

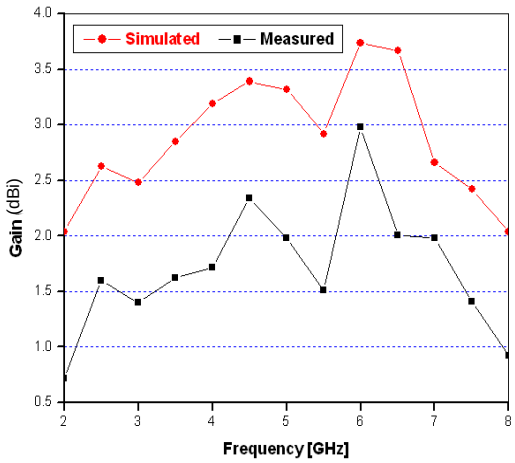

Figure 23. Simulated and measured gain of the proposed antenna.

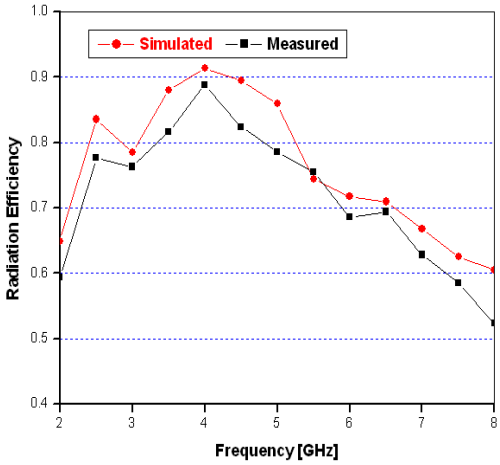

Figure 24. Simulated and measured radiation efficiency of the proposed antenna.

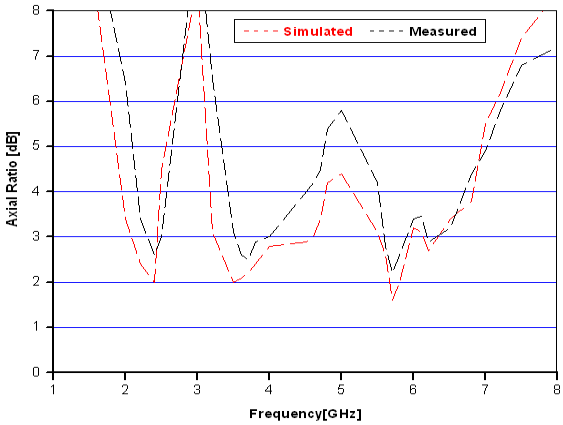

Figure 25. Simulated and Measured AR (axial ratio) (along $\theta = 87°$ and $\Phi = -89°$) of the proposed antenna.

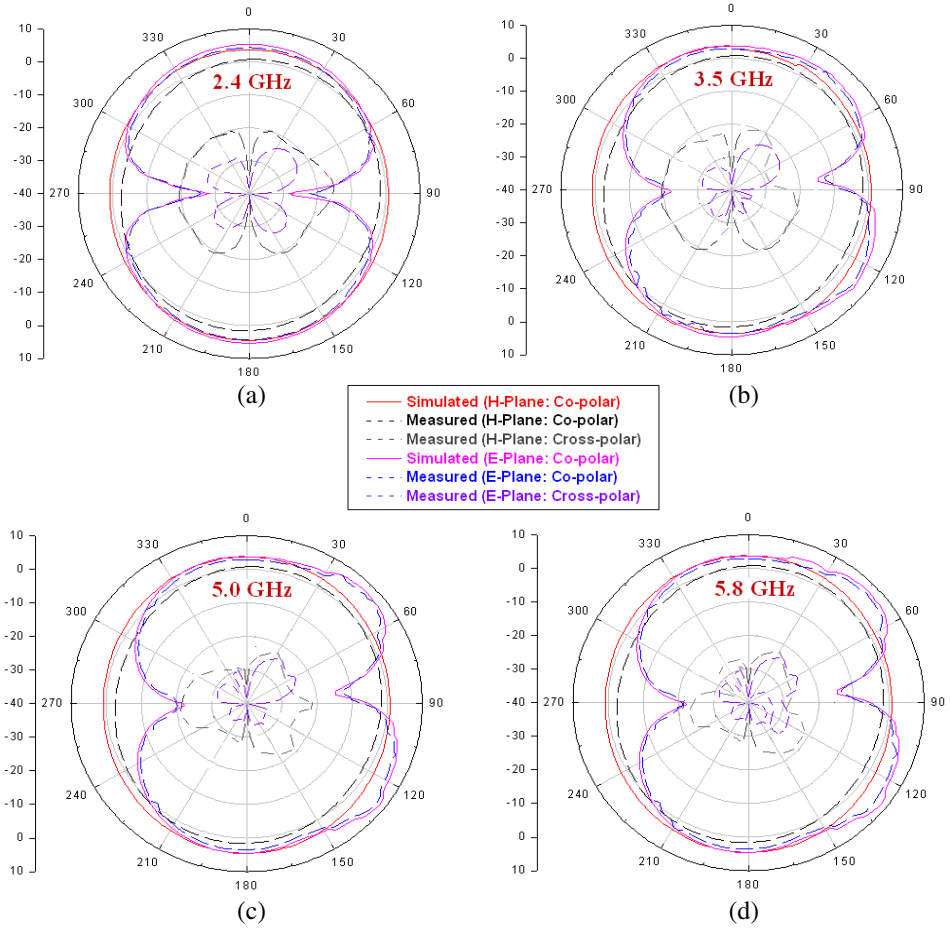

Figure 26. Simulated and Measured E & H-plane radiation patterns of the proposed antenna at; (a) 2.4 GHz, (b) 3.5 GHz, (c) 5.0 GHz and (d) 5.8 GHz.

88.7% to 52.8% in measurement. The measured radiation efficiencies of 72.8%, 82.4%, 79.2% and 72.1% are observed for 2.4, 3.5, 5 and 5.8 GHz WLAN and WiMAX frequency bands. So it is observed that the efficiency stays above 70% in all the operating bands, showing decreasing trend in radiation efficiency with increase in frequency.

The axial ratio (AR) of the proposed antenna is measured with the help of Antenna Measurement System in conjunction with a Vector Network Analyzer inside an anechoic chamber. For obtaining the best performance regarding maximum ARBW (Axial ratio bandwidth) as shown in Figure 25, the measurement system is set up along the directions of $\theta = 87^\circ$ and $\Phi = -89^\circ$. The simulated AR stays less than 3 dB from 2.10–2.51 GHz (17.8%), 3.25–4.72 GHz (36.9%) and 5.52–6.10 GHz (9.9%) centered at 2.31, 3.99 and 5.8 GHz respectively. The measured ARBW (axial ratio bandwidth) is slightly less than the simulated ARBW at 13.6% (2.25–2.58 GHz), 23.8% (3.29–4.18 GHz) and 6.4% (5.61–5.98 GHz) as shown in Figure 25. The wideband CP is achieved by optimizing the strip between patch and SRR's and inner and outer rings of rectangular SRR's, which are responsible for creating alternate current paths that produces two orthogonal degenerate modes on the patch of the proposed structure.

The simulated and measured E-plane and H-plane radiation patterns for the rectangular SRR loaded octagonal shape antenna at 2.4 GHz, 3.5 GHz, 5.0 GHz and 5.8 GHz are shown in Figure 26. The radiation patterns are plotted in both co- and cross-polarizations. From Figure 26, it is seen that the E-plane radiation patterns are dipole-like radiation pattern whereas the H-plane radiation patterns resemble omnidirectional ones. The cross-polarization levels less than -15 dB are achieved in both E & H-plane patterns for all the frequency bands of interest. There is a good agreement between the measured and simulated radiation patterns for E and H planes for co- and cross-polarizations with a slight difference caused by assembly misalignments.

As shown in Figure 26, most of the radiation patterns seem to be reasonably stable with respect to frequency. The E-plane pattern shows a pinch-off along the end fire directions ($\theta = \pm 90^\circ$) at lower frequencies (below 3 GHz), because of the increased cross polarization at these frequencies but not evident for higher frequencies.

Tables 2 and 3 represent the comparison of antenna characteristics, such as gain, radiation efficiency, bandwidth and size, between the fabricated proposed antenna and other metamaterial loaded antennas for WLAN frequency band (2.4 & 5 GHz) and WiMAX frequency band (3.5 GHz) [35].

Table 2. Comparision for 2.4 GHz.

Parameter	Proposed antenna	Ref. [23]	Ref. [25]
Bandwidth (in %)	4.5	3.28	3.68
Gain (in dBi)	1.58	2.85	−1.04
Radiation Efficiency (in %)	72.8	91.8	72.5
Antenna Size (in mm^3)	38×38×1.6	49×49×6	52.6×30×1

Table 3. Comparision for 3.5 & 5 GHz.

Parameter	Proposed antenna	Ref. [23]	Ref. [25]
Bandwidth (in %)	51.1	6.44	2.88
Gain (in dBi)	1.75	5.12	1.08
Radiation Efficiency (in %)	82.4	97.6	76.4
Antenna Size (in mm^3)	38×38×1.6	49×49×6	52.6×30×1

4. CONCLUSION

A compact SRR loaded octagonal shape antenna fed by a microstrip line is designed, simulated and implemented for validating the experimental design. The operating frequencies of the proposed antenna are 2.4, 3.5, 5.0 and 5.8 GHz, which meet the WLAN and WiMAX requirements. At these frequencies, antenna characteristics are obtained with good impedance matching. A prototype of the proposed SRR loaded antenna is fabricated on an FR4 substrate which can easily be integrated with wireless terminal devices. The proposed antenna represents omnidirectional radiation characteristics in the H-plane for the frequency bands of interest, as requirement for the wireless applications. The proposed antenna is intended for the use in WLAN and WiMAX wireless applications.

REFERENCES

1. Chakraborty, M., B. Rana, P. Sarkar, and A. Das, "Size reduction of microstrip antenna with slots and defected ground structure," *International Journal of Electronics Engineering*, Vol. 4, No. 1, 61–64, 2012.
2. . Elftouh, H., N. A. Touhami, M. Aghoutane, S. El Amrani, A. Tazon, and M. Boussouis, "Miniaturized microstrip patch antenna with defected ground structure," *Progress In Electromagnetics Research C*, Vol. 55, 25–33, 2014.
3. Elftouh, H., N. A. Touhami, and M. Aghoutane, "Miniaturized microstrip patch antenna with spiral defected microstrip structure," *Progress In Electromagnetics Research Letters*, Vol. 53, 37–44, 2015.
4. Mahatthanajatuphat, C., S. Saleekaw, and P. Akkaraekthalin, "A rhombic patch monopole antenna with modified Minkowski fractal geometry for UMTS, WLAN, and mobile WIMAX application," *Progress In Electromagnetics Research*, Vol. 89, 57–74, 2009.
5. Shrestha, S., S. R. Lee, and D.-Y. Choi, "New fractal-based miniaturized dual band patch antenna for rf energy harvesting," *International Journal of Antennas and Propagation*, Vol. 2014, 2014.
6. Gianvittorio, J. P. and Y. Rahmat-Samii, "Fractal antennas: A novel antenna miniaturization technique, and applications," *IEEE Antennas and Propagation Magazine*, Vol. 44, No. 1, 20–36, 2002.
7. . Suganthi, S., S. Raghavan, and D. Kumar, "Miniature fractal antenna design and simulation for wireless applications," *IEEE RAICS*, 57–61, 2011.
8. Liua, W.-C., C.-M. Wua, and N.-C. Chu, "A compact low profile dual-band antenna for WLAN and WAVE applications," *AEU Int. J. Electron. C*, Vol. 66, 467–471, 2012.
9. Saraswat, R. K. and M. Kumar, "A frequency band reconfigurable uwb antenna for high gain applications," *Progress In Electromagnetics Research B*, Vol. 64, 29–45, 2015.
10. Kumar, M., A. Basu, and S. K. Koul, "UWB printed slot antenna with improved performance in time and frequency domains," *Progress In Electromagnetics Research C*, Vol. 18, 197–210, 2011.
11. Kumar, M., A. Basu, and S. K. Koul, "Circuits and active antennas for ultrawideband pulse generation and transmission," *Progress In Electromagnetics Research B*, Vol. 23, 251–272, 2010.
12. Su, S.-W., "Compact four loop antenna system for concurrent, 2.4 and 5 GHz WLAN operation," *Microw. Opt. Technol. Lett.*, Vol. 56, No. 1, 208–215, 2014.
13. Chien, H. Y., C. Y. D. Sim, and C. H. Lee, "Dual band meander monopole antenna for WLAN operation in laptop computer," *IEEE Antennas Wirel. Propag. Lett.*, Vol. 12, 694–697, 2013.
14. Huang, C.-Y. and E.-Z. Yu, "A slot monopole antenna for dual band WLAN applications," *IEEE Antennas Wirel. Propag. Lett.*, Vol. 10, 500–502, 2011.
15. Ghatak, R., R. K. Mishra, and D. R. Poddar, "Perturbed Sierpinski carpet antenna with CPW feed for IEEE 802.11a/b WLAN application," *IEEE Antennas Wirel. Propag. Lett.*, Vol. 7, 742–745, 2008.
16. Xu, Y., Y.-C. Jiao, and Y.-C. Luan, "Compact CPW-fed printed monopole antenna with triple band characteristics for WLAN/WiMAX applications," *Electron. Lett.*, Vol. 48, No. 24, 1519–1520, 2012.
17. Sim, C. Y. D., H. D. Chen, K. C. Chiu, and C. H. Chao, "Coplanar waveguide fed slot antenna for wireless local area network/worldwide interoperability for microwave access applications," *IET Microw. Antenna Propag.*, Vol. 6, No. 14, 1529–1535, 2012.
18. Basaran, S. C., U. Olgun, and K. Sertel, "Multiband monopole antenna with complementary split ring resonators for WLAN and WiMAX applications," *Electron. Lett.*, Vol. 49, No. 10, 636–638, 2013.
19. Zhang, X.-Q., Y.-C. Jiao, and W.-H. Wang, "Compact wide tri-band slotantenna for WLAN/WiMAX applications," *Electron. Lett.*, Vol. 48, No. 2, 64–65, 2012.
20. Li, X., X.-W. Shi, W. Hu, P. Fei, and J.-F. Yu, "Compact triband ACS fed monopole antenna employing open ended slots for wireless communication," *IEEE Antennas Wirel. Propag. Lett.*, Vol. 12, 388–391, 2013.

21. Liu, P., Y. Zou, B. Xie, X. Liu, and B. Sun, "Compact CPW fed tri band printed antenna with meandering split ring slot for WLAN/WiMAX applications," *IEEE Antennas Wirel. Propag. Lett.*, Vol. 11, 1242–1244, 2012.
22. Xu, H.-X., G.-M. Wang, J.-G. Liang, M.-Q. Qi, and X. Gao, "Compact circularly polarized antennas combining meta-surfaces and strong space-filling meta-resonators," *IEEE Trans. Antennas Propag.*, Vol. 61, No. 7, 3442–3450, 2013.
23. Xu, H.-X., G.-M. Wang, and M.-Q. Qi, "A miniaturized triple-band metamaterial antenna with radiation pattern selectivity and polarization diversity," *Progress In Electromagnetics Research*, Vol. 137, 275–292, 2013.
24. Xu, H.-X., G.-M. Wang, M.-Q. Qi, C.-X Zhang., J.-G. Liang, J.-Q. Gong, and Y.-C. Zhou, "Analysis and design of two-dimensional resonant-type composite right/left-handed transmission lines with compact gain-enhanced resonant antennas," *IEEE Trans. Antennas Propag.*, Vol. 61, No. 2, 735–747, 2013.
25. Xu, H.-X., G.-M. Wang, Y.-Y. Lv, M.-Q. Qi, X. Gao, and S. Ge, "Multi frequency monopole antennas by loading metamaterial transmission lines with dual-shunt branch circuit," *Progress In Electromagnetics Research*, Vol. 137, 703–725, 2013.
26. Basaran, S. C. and Y. E. Erdemli, "A dual band split ring monopole antenna for WLAN applications," *Microw. Opt. Technol. Lett.*, Vol. 51, No. 11, 2685–2688, 2009.
27. Dong, Y., H. Toyao, and T. Itoh, "Design and characterization of miniaturized patch antennas loaded with complementary split ring resonators," *IEEE Trans. Antennas Propag.*, Vol. 60, No. 2, 772–785, 2012.
28. Xiong, J., H. Li, Y. Jin, and S. He, "Modified TM020 mode of a rectangular patch antenna partially loaded with metamaterial for dual band applications," *IEEE Antennas Wireless Propag. Lett.*, Vol. 8, 1006–1009, 2009.
29. Zhu, J. and G. V. Eleftheriades, "Dual band metamaterial inspired small monopole antenna for WiFi applications," *Electron. Lett.*, Vol. 45, No. 22, 1104–1106, 2009.
30. Computer Simulation Technology–CST (Microwave Studio MWS) Version-2014.
31. Smith, D. R., S. Schultz, P. Markos, and C. M. Soukoulis, "Determination of negative permittivity and permeability of metamaterials from reflection and transmission coefficients," *Phys. Rev. B*, Vol. 65, 195104–9, 2002.
32. Chen, H., J. Zhang, Y. Bai, Y. Luo, L. Ran, Q. Jiang, and J. A. Kong, "Experimental retrieval of the effective parameters of metamaterials based on a waveguide method," *Opt. Express*, Vol. 14, No. 26, 12944–12949, 2006.
33. Saha, C. and J. Y. Siddiqui, "Versatile CAD formulation for estimation of the resonant frequency and magnetic polarizability of circular split ring resonators," *Int. J. RF Microw. Comput. Aided Eng.*, Vol. 21, 432–438, 2011.
34. Ray, K. P. and G. Kumar, "Determination of resonant frequency of microstrip antennas," *Microw. Opt. Technol. Lett.*, Vol. 23, 114–117, 1999.
35. Rahimi, M., F. B. Zarrabi, R. Ahmadian, Z. Mansouri, and A. Keshtkar, "Miniaturization of antenna for wireless application with difference metamaterial structures," *Progress In Electromagnetics Research*, Vol. 145, 19–29, 2014.